J Nanopart Res (2013) 15:1688
DOI 10.1007/s11051-013-1688-0

RESEARCH PAPER

Synthesis of Ag@ZnO core–shell hybrid nanostructures: an optical approach to reveal the growth mechanism

Ezequiel R. Encina · Manuel A. Pérez · Eduardo A. Coronado

Received: 8 February 2013 / Accepted: 29 April 2013

Abstract In this study, Ag@ZnO core–shell hybrid nanostructures (HNs) have been prepared by means of a very simple chemical methodology. In addition, their morphology and extinction properties have been characterized. It was found that the HNs consist in almost spherical Ag nanoparticle cores (mean diameter 56 nm) surrounded by a thin shell formed by small ZnO nanoparticles (mean size 6 nm). The changes in the extinction spectra during the formation of the hybrid nanostructures have been rationalized using electrodynamics simulations applying Mie theory for coated spheres along with the effective medium theory to describe the dielectric constant of the shell. By assuming a formation and growth mechanism of the shell, it was found that these simulations describe not only qualitatively but also quantitatively the changes in the extinction spectra.

Keywords Plasmons · Noble metal · Semiconductor · Core shell · Hybrid nanostructures

Electronic supplementary material The online version of this article (doi:10.1007/s11051-013-1688-0) contains supplementary material, which is available to authorized users.

E. R. Encina · M. A. Pérez · E. A. Coronado (✉)
Departamento de Fisicoquímica, Facultad de Ciencias Químicas, INFIQC, Universidad Nacional de Córdoba, 5000 Córdoba, Argentina
e-mail: coronado@fcq.unc.edu.ar

Introduction

Heterogeneous structures composed of a noble metal and a semiconductor nanomaterial (hybrid nanostructures) have attracted considerable inerest during the recent years especially because of the possibility that this peculiar type of systems offers to design materials with novel and unique physical chemistry properties (Costi et al. 2010; Cohen-Hoshen et al. 2012; Khanal et al. 2012; Kamat 2012; Linic et al. 2011). As isolated systems, the optical properties of semiconductor quantum dots (QDs) and noble metal nanoparticles (NPs) are characterized by excitons and plasmons, respectively. In both cases, the required wavelengths to produce such excitations are governed mainly by the nanoparticle nature, size, shape, and local environment (Pesika et al. 2003; Zhang et al. 2010a, b; Kelly et al. 2003; Encina and Coronado 2007). Therefore, the development of synthetic methodologies to generate QDs and NPs with a large control over its structural parameters is crucial to exploit the properties that merge at the nanoscale in a given device (Meulenkamp 1998; Hartlieb et al. 2007; Segets et al. 2009; Layek et al. 2012; Rycenga et al. 2011; Jones et al. 2011). Hybrid nanostructures exhibit, in addition, properties that may differ from those observed for their separated building blocks as a consequence of the interaction between them. This interaction can be, in turn, modulated by a fine control over the HN composition and architecture. For instance, the direct contact between QDs and NPs can lead to interfacial charge

Published online: 16 May 2013

transfer processes that are of paramount importance in highly relevant topics such as photocatalytic reactions and light energy conversion (Wood et al. 2001; Subramanian et al. 2003; Jakob et al. 2003; Lee et al. 2011). Alternatively, if QDs and NPs are arranged in close proximity within a given HN, then energy transfer processes may occur, according to, for example, the mechanisms described by Förster resonance energy transfer (FRET) and Nanometal surface energy transfer (NSET) (Chen et al. 2008; Munechika et al. 2010; Torimoto et al. 2011; Li et al. 2011). For instance, the emission properties of a given QD can be enhanced or quenched by tuning the resonance wavelength of plasmons according to the emission wavelength, as well as by controlling the separation between QDs and NPs (Viste et al. 2010). The distinct ways of combining the structure parameters bring the possibility of designing a wide variety of HNs to explore new optical phenomena at the nanoscale that might result from plasmons and excitons interactions in a single object.

From the synthetic point of view, several strategies have been developed and implemented for the preparation of HNs. For instance, Zhang et al. (2010a, b) have reported a general nonepitaxial growth strategy which achieves precise control over the morphologies of Au–CdS, Au–CdSe, Au–CdTe, Au–PbS, and Au–ZnS core–shell HNs. Another facile and general strategy for the synthesis of water-dispersible Au–MS core–shell HNs (M = Zn, Cd, Ag, or Ni) have been developed by Sun et al. (2009). Au–TiO_2 (Zhang et al. 2011a, b) as well as Ag–TiO_2 (Qi et al. 2011) core–shell nanocomposites had also been successfully synthesized. It is important to remark that, among the wide variety of semiconductor materials studied, ZnO has attractive optical properties and outmatches Cd compounds QDs when cost, chemical stability, and safety are being taken into account (Hartlieb et al. 2007; Segets et al. 2009). In this respect, Udawatte et al. (2011) modified ZnO QDs with preformed Au NPs protected with bifunctional glutathione ligand and demonstrated that thiolate-protected Au NPs can significantly enhance the charge separation by extracting electrons from the photoexcited ZnO, and consequently, improve the photocatalytic activity of the composites. In this regard, several types of Ag/ZnO HNs have been prepared by applying mainly solvothermal methods. The majority of the structures obtained in this way consist of large (several hundreds of nm) ZnO particles *decorated* with Ag NPs (Zheng et al. 2007; Fan et al. 2009; Mahanti and Basak 2012; Yoo et al. 2012; Sun et al. 2012). In general, it is found that the presence of Ag NPs on the surface of ZnO structures promotes the separation of photogenerated electron–hole pairs and thus enhances the photocatalytic and SERS activity (Georgekutty et al. 2008; Lu et al. 2008; Zheng et al. 2008; Lin et al. 2009; Shan et al. 2007; Cheng et al. 2010; Richter et al. 2010; Xu et al. 2011). However, there exist only a few studies concerning the synthesis and optical characterization of Ag@ZnO core–shell HNs. In this respect, Liu et al. (2012a, b) have fabricated novel worm-like Ag@ZnO core–shell heterostructural composites using a two-step chemical method, and found that these metal core–semiconductor shell composites are photocatalytically active and useful to promote light induced electron transfer reactions. In a recent study, Aguirre et al. (2011) have reported a new synthetic methodology for Ag@ZnO core–shell HNs by means of a simultaneous reduction of Ag^+ ions and zinc acetate hydrolysis in *N*,*N* dimethylformamide at room temperature. The characterizations of emission and photocatalytic properties reveal en efficient electron transfer from ZnO to Ag.

Electrodynamics modeling of the optical properties of HNs, taking into account structural information obtained from morphologic characterization, is of great importance to achieve further insight of the observed phenomena. As far as we know, electrodynamics modeling of this type of HNs has been carried out in some studies mainly focused in interpreting the extinction spectra of Au@Cu_2O core–shell HNs. For instance, Liu et al. (2012a, b) have prepared Au@Cu_2O core–shell HNs with tunable thickness by controlling epitaxial growth of Cu_2O on as-prepared gold NPs in aqueous solution. In this study, the authors employed an analytic model based on an approximate Mie's theory, within the framework of the electrostatic approximation, to interpret the optical features of the Au@Cu_2O core–shell HNs. Another robust wet chemistry approach, which involves the controllable growth of a polycrystalline Cu_2O nanoshell surrounding a Au NP core, has been developed by Zhang et al. (2011a). In this study, the complexity of extinction of spectral line shapes and the geometry-dependent optical tunability of the Au@Cu_2O HNs has been interpreted using Mie theory calculations for coated spheres.

Motivated, in part, by the above reasons, a simple alternative chemical method that allows one to synthesize Ag@ZnO core–shell HNs has been implemented in the present study. The obtained HNs are mainly composed by nearly spherical Ag NPs surrounded by a relatively thin shell of ZnO QDs. In addition, we have performed electrodynamics simulations, based on Mie theory for coated spheres combined with effective medium theories to describe the dielectric constant of the shell, to gain insight into the changes observed in the extinction spectra of the HNs prepared. Interestingly, we demonstrate that by combining the TEM characterization of the samples with the above mentioned electrodynamics theoretical approach, it is possible to describe in a consistent way the nucleation and growth mechanism of the HNs.

Experimental section

Materials

Sodium citrate ($Na_3C_6H_5O_7$, Mallinckrodt), silver nitrate ($AgNO_3$, Carlo Erba), zinc nitrate ($Zn(NO_3)_2{\cdot}6H_2O$, Anedra), potassium hydroxide (K(OH), Cicarelli), and ethanol (anhydrous, Dorwil) were used as received without further purification. Aqueous solutions were prepared with ultrapure water (18.2 mΩ resistivity).

ZnO QDs

In order to correlate ZnO QDs optical properties as isolated nano-objects with those observed for HNs, ZnO QDs were produced by using a simple method. 25 μL of 0.02 M KOH ethanolic solution was added to 5 mL of 0.0001 M $Zn(NO_3)_2$ ethanolic solution to obtain a hereafter referred as "reactive solution," which was kept at 70 °C for 30 min and, finally cooled and stored at room temperature. Reactive solutions at room temperature were periodically characterized by UV–Visible spectroscopy to monitor the formation and growth of ZnO QDs.

Ag NPs

The synthesis of Ag NPs was performed by adapting the Turkevich method. Aliquots of 0.1 M sodium citrate aqueous solution (0.25 mL) and of 0.01 M silver nitrate aqueous solution (2.5 mL) were added to 97.25 mL of boiling water under vigorous stirring, to give a green–yellowish color which characterizes Ag NPs in suspension. The system was kept at boiling temperature for 40 min to complete the reaction, and then it was cooled at room temperature. Ag NPs were purified by performing centrifugation of 10 mL of the aqueous suspension of Ag NPs for 7 min at 5,000 rpm. The resulting precipitate was redispersed in 10 mL of ethanol (dispersion A). Dispersion A was separated in two aliquots (B and C) of 5 mL. Aliquot B was heated at 70 °C for 30 min and then cooled and stored at room temperature for control, while aliquot C was used for the synthesis of the HNs.

Ag@ZnO hybrid nanostructures

HNs were prepared by implementing a new synthetic methodology that resembles the one reported by Lee et al. (2008). 25 μL of 0.02 M KOH and 0.05 mL of 0.01 M $Zn(NO_3)_2$ ethanolic solutions were added to aliquot C, which was kept at 70 °C for 30 min and, was finally cooled and stored at room temperature. Using this procedure, it is expected that the surface of Ag NP favors heterogenous nucleation of ZnO during the zinc oxide formation.

Optical and morphologic characterizations

UV–Vis spectroscopy characterization was carried out by using a Shimazdu UV-1700 PharmaSpec spectrophotometer with a 1-cm quartz cell at room temperature. Transmission electron microscopy (TEM) images were obtained using a JEM-JEOL 1120 EXII instrument under an accelerating voltage of 80 kV. Samples were prepared by seeding a drop ($\sim$20 μL) of the colloidal dispersion to be characterized onto a holey carbon/Formvar-coated copper TEM grid (100 mesh).

Results and discussion

Synthesis and characterization of ZnO QDs

Figure 1a shows the spectral evolution of a reactive solution during the formation and growth of ZnO QDs. In general, it is observed that the sample is transparent in the whole UV–NIR interval exhibiting an absorption onset at shorter wavelengths values of approximately

at 360 nm. This is the typical response expected for colloidal suspension of ZnO QDs, where the energy absorption in the UV range is attributed to the creation of excitons. It could also be appreciated that the absorption edge shifts toward longer wavelengths (lower energies) with time, which qualitatively indicates a decrease in the semiconductor band gap, which in turn is associated with the increase of the average size of the QDs.

The relationship between the absorption coefficient α near the absorption edge and the optical band gap (E_g) for direct interband transitions, as that occurs in ZnO, is given by

$$(\alpha hv)^2 = A(hv - E_g), \tag{1}$$

where A is a constant, and hv is the photon energy (Zhang et al. 2010a, b). Thus, the E_g values can be obtained by extrapolating the linear portion of a plot $(\alpha hv)^2$ versus hv to $\alpha = 0$. Spectral data shown in Fig. 1a are represented in the inset according to Eq. (1). In this way, the interception of the linear portion of each curve with the abscissa axis provides a good estimation of E_g. Table 1 summarizes the E_g values obtained by means of this procedure.

The effective mass model for spherical particles provides a useful tool to account for the relationship between E_g and QD size, where such dependence can be approximated by (Brus 1984):

$$E_g \cong E_{bulk} + \frac{h^2}{2S^2}\left(\frac{1}{m_e^*} + \frac{1}{m_h^*}\right) - \frac{1.8e^2}{2\pi c\, \varepsilon_0 S} \tag{2}$$

In Eq. (2) E_{bulk} is the bulk band gap (3.37 eV at room temperature), m_e^* is the effective mass of the electrons in the conduction band, m_h^* is the effective mass of the holes in the valence band, h is Planck's constant, ϵ is the relative permittivity, ε_0 is the permittivity of free space, e is the electron charge, and S is the QD diameter. Given that Eq. (2) can be used to determine the QD diameter if E_g value is known, the E_g values estimated above were used to obtain the QD diameter at different aging times. The values used for m_e^*, m_h^*, and ϵ in the calculations were 0.24, 0.45, and 3.7, respectively, according to the values employed by Brus (1984). The S values listed in Table 1 correspond to the average QD size of the ZnO colloidal suspension, and the trend observed clearly indicates that the QDs size increases with aging time. Figure 1b shows a representative TEM micrography of the ZnO QDs

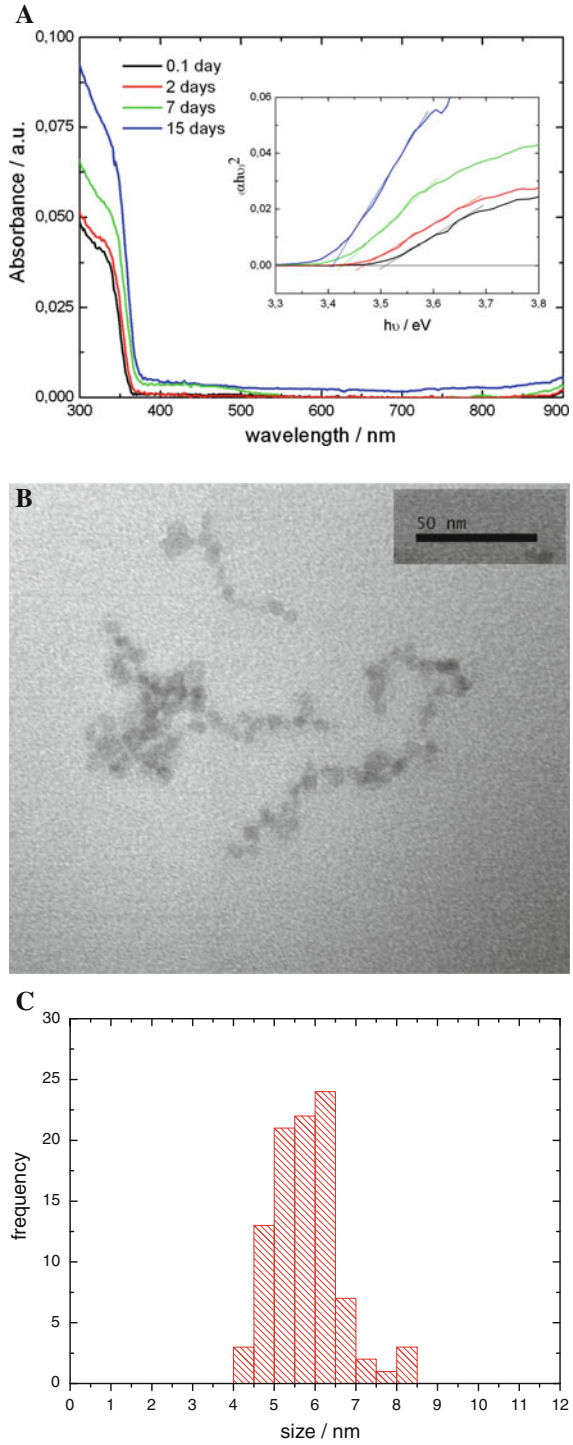

Fig. 1 **a** Spectral evolution of a reactive solution during the formation and growth of ZnO QDs. The inset shows the data plotted according to Eq. (1). **b** TEM image representative of the ZnO QDs after 15 days aging along with **c** the respective size distribution histogram

Table 1 Comparison between the optical band gap E_g and diameter S values obtained for the synthesized ZnO QDs using Eqs. (1) and (2), respectively, for different aging times

Aging time/days	0.1	2	7	15
E_g/eV	3.51	3.46	3.43	3.41
S/nm	4.0	5.0	5.6	6.0

sample after 15 days aging, where the QD's average diameter is around 6 nm (see the histogram in Fig. 1c), in good agreement with the mean size determined using Eq. (2).

Synthesis and characterization of Ag NPs

Figure 2a shows the evolution of the normalized extinction spectra of Ag NPs colloidal suspension as time elapses. The main feature of all of these spectra is a peak centered at 435 nm, which is attributed to the localized surface plasmon resonance (LSPR) of Ag NPs, where the spectral position of this resonance is determined by their size and shape distribution. Although there is a slight LSPR broadening, the spectral position of the peak does not change significantly with time, which suggests that the size and shape distribution remains practically unchanged even after a relatively long period (15 days). The slight increase of the extinction intensity for $\lambda > 600$ nm with elapsing time can be attributed to some extent to the formation of a small proportion of Ag NPs aggregates. Besides this observation, the important information to extract from the results shown in Fig. 2a is that the Ag NPs display a good stability in ethanolic media. Figure 2b shows a TEM micrograph representative of the Ag NPs sample dispersed in ethanol after 15 days' aging. Although the presence also of some elongated particles is observed,the presence of nearly spherical NPs with a mean diameter of 56 nm is predominant (see histogram in Fig. 2c).

Synthesis and characterization of Ag@ZnO HNs

Figure 3a shows the evolution of the normalized extinction spectra during the formation of ZnO QDs in a reactive solution that contains Ag NPs. The main change observed in this case is a redshift of the LSPR position from 435 to 455 nm after 15 days of reaction time. In addition, the absence of any increase of the extinction intensity for $\lambda > 600$ nm suggests that the formation of Ag NPs aggregates in the presence of ZnO QDs precursors is unfavored. This redshift of the LSPR cannot be attributed to the formation of Ag NPs aggregates because it has been demonstrated in a previous study (Encina and Coronado 2010) that the plasmon resonances of these nanostructures occurs at longer wavelengths ($\lambda \geq 600$ nm) than that corresponding to isolated Ag NPs. Besides, changes of the shape and size distribution of the Ag NPs induced by adding Zn^{2+} and OH^- ions to the system are fairly unlikely. In addition, the formation of ZnO QDs from its precursors is not inhibited by the presence of Ag NPs. Moreover, it is reasonable to suggest that the redshift of the LSPR is a consequence of the interaction between Ag NPs and ZnO QDs. Along of this line of thinking, the LSPR redshift can be consistently explained in terms of the increase of the dielectric constant of the surroundings of Ag NPs caused by the proximity of ZnO QDs to NPs' surface. Note that the Ag NPs are surface functionalized with citrate ions, which come from the synthetic method employed and provide stability to the NPs dispersion. These citrate groups are able to act as linkers between Ag and ZnO, as the chemical interaction between ZnO and COOH groups has been already demonstrated (Taratula et al. 2006; Cho et al. 2009; Lenz et al. 2009; Chen et al. 2010). Figure 3b shows some representative TEM micrographs of the Ag@ZnO sample after 15 days' aging. HNs formed by a Ag NP core surrounded by a well-defined shell of small ZnO QDs can be clearly observed. In addition, the presence of some ZnO QDs agglomerates can also be observed, and therefore, it is quite likely that nucleation and growth of ZnO QDs are taking place simultaneously in an homogeneous as well as in a heterogeneous process. The homogeneous process corresponds to the nucleation and growth of ZnO from the bulk solution, while the heterogeneous one is related to the nucleation and growth of ZnO QDs already attached to surface of the Ag NPs via interaction with the COOH groups of citrate molecule. Therefore, the formation of Ag@ZnO core–shell HNs explains qualitatively the redshifts of the LSPR observed in Fig. 3a. The histogram shown in Fig. 3c represents the size distribution of ZnO QDs that are attached to the Ag NPs surface and form the shell of the HNs. Upto 15 days' aging, it is observed that the HNs remain as a stable colloidal dispersion in solution. For aging times of 20 days or longer, increasing amounts of precipitate are observed in the test tube

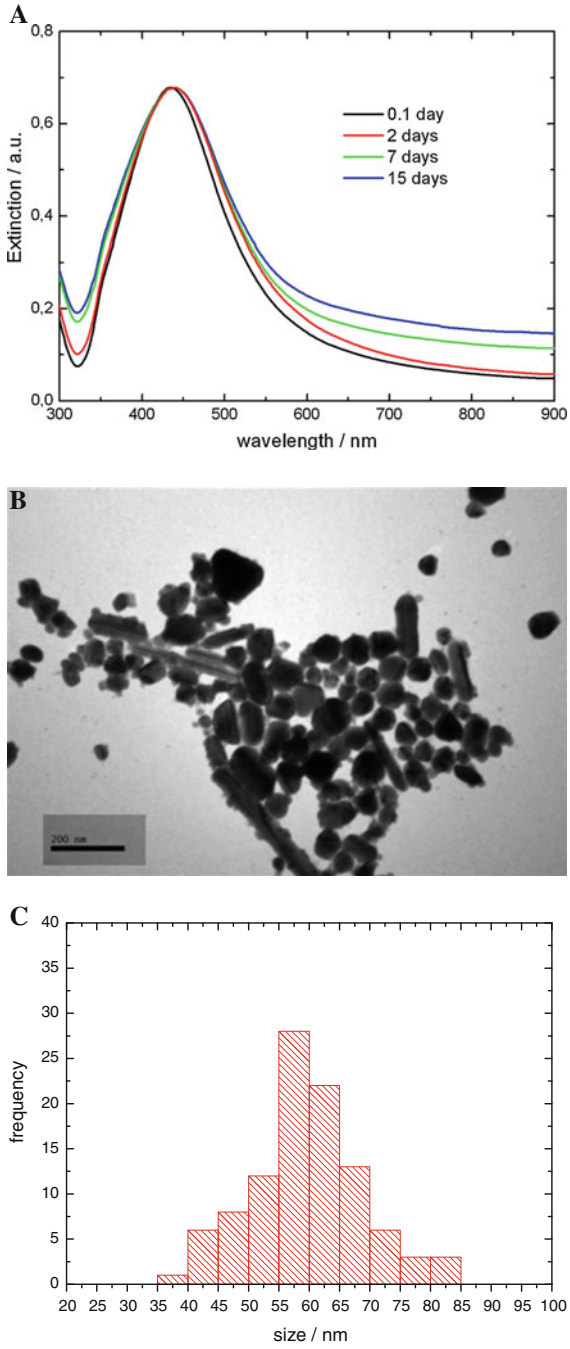

Fig. 2 **a** Spectral evolution of the normalized extinction spectra of the colloidal suspension of Ag NPs dispersed in ethanol. **b** TEM image representative of the Ag NPs after 15 days' aging along with **c** the respective size distribution histogram

that contains the HNs, which can be dispersed by stirring the solution. In addition, it is important to mention that the low concentrations of Ag NPs and ZnO precursors used in this study are necessary for the success of the synthesis. HNs with morphologies much more complex than the core–shell type were obtained when higher concentrations of Zn^{2+} were employed in the synthesis (see Fig. 1S in Supporting Information).

The net effect of the formation of ZnO in the presence of Ag NPs gives rise to important changes in the optical properties as summarized in Fig. 4. Black and red curves depict the extinction spectra of a colloidal dispersion of ZnO QDs and Ag NPs, respectively. If there were no interaction between ZnO and Ag nanoparticles, then the extinction spectrum that would be obtained by mixing ZnO and Ag colloidal suspensions should be given by the sum of their individual spectra, which corresponds to the blue curve depicted in Fig. 4. However, the spectrum of the Ag@ZnO sample (green curve) shows significant differences with respect to the blue curve, particularly the spectral position of the LSPR redshifts 20 nm with respect to the colloidal dispersion of Ag NPs. This redshift could be attributed to an increase of the dielectric constant around the Ag NPs that, in principle, is consistent with the formation of a ZnO shell.

Modeling of the extinction spectra of HNs

In order to give a more rigorous insight into the observed phenomena, we have performed classical electrodynamics simulations based on Mie theory for coated spheres as formulated by Aden and Kerker (Bohrem and Huffman 1983). In our case, it is assumed that light interacts with the structure schematized in Fig. 5, which consists in a spherical Ag core of diameter D surrounded by a uniform shell of thickness S immersed in ethanol. Note that in the idealized structure employed to describe the synthesized HNs not all of the shell is occupied by ZnO, which aims, as much as possible, to capture in a simple model the characteristic observed in the TEM images (Fig. 3b).

A very important aspect to consider in these simulations is to assign a value to the dielectric constant of the shell for each wavelength. This assignment must be as correct as possible if it is presumed that theoretical results gives not only a qualitative but also a quantitative description of measured extinction spectra. In this respect, the following relatively simple average dielectric function,

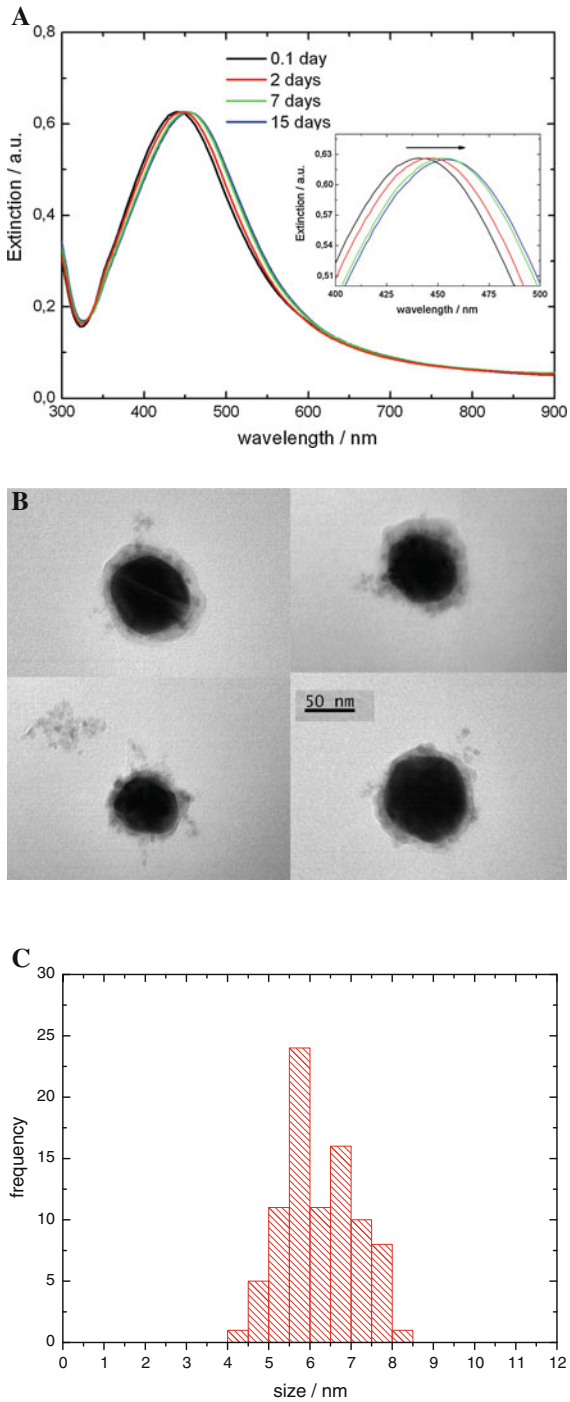

Fig. 3 **a** Spectral evolution of the normalized extinction spectra of the colloidal suspension of Ag@ZnO HNs dispersed in ethanol. **b** TEM images representatives of the Ag@ZnO HNs after 15 days' aging along with **c** the ZnO QDs' size distribution histogram

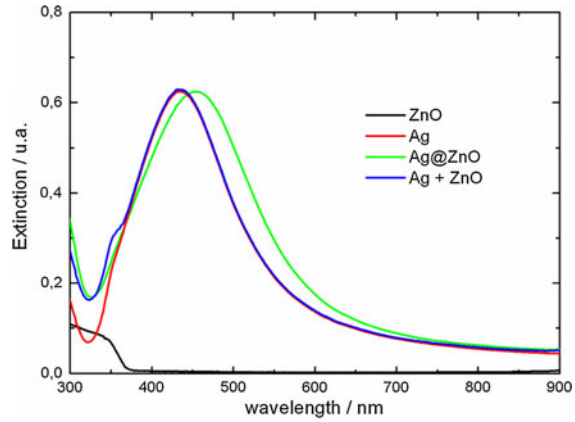

Fig. 4 Comparison between the extinction spectrum of the Ag@ZnO HNs colloidal dispersion and the spectrum resulting from the sum of the Ag NPs and ZnO QDs individual extinction spectra

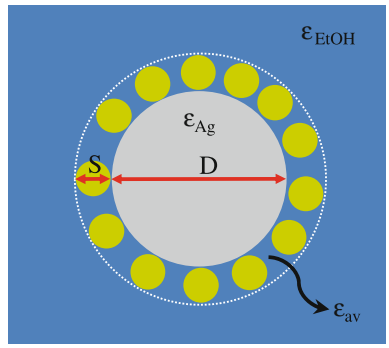

Fig. 5 Scheme of the nanostructure model used in electrodynamics simulations to represent the Ag@ZnO core–shell HNs

$$\varepsilon_{\mathrm{av}} = \varepsilon_{\mathrm{m}}\left[1 + \frac{3f\left(\frac{\varepsilon-\varepsilon_{\mathrm{m}}}{\varepsilon+2\varepsilon_{\mathrm{m}}}\right)}{1-f\left(\frac{\varepsilon-\varepsilon_{\mathrm{m}}}{\varepsilon+2\varepsilon_{\mathrm{m}}}\right)}\right], \tag{3}$$

first derived by Maxwell and Garnet and often called *effective medium* dielectric function, is a suitable function for the present purposes (Bohrem and Huffman 1983). Equation (3) allows us to determine the dielectric constant $\varepsilon_{\mathrm{av}}$ of a medium with spherical inclusions, where ε_{m} is the dielectric constant of the medium, ε is the dielectric constant of the inclusions, and the parameter f is the volume fraction occupied by the inclusions. In our case, the medium is ethanol ($\varepsilon_{\mathrm{m}} = 1.85$) and the inclusions are the spherical ZnO QDs. The values reported by Postava et al. (2000) for

ε_{ZnO} were introduced into Eq. (3) to obtain the wavelength-dependent ε_{av} values.

Thus, to model the measured spectra with the methodology described above, several parameters are required:

- the average Ag NPs size (determined by TEM and the histogram shown in Fig. 2c);
- the Ag dielectric constant (taken from Palik (1985));
- the average thickness S of the shell (determined by TEM and the histogram shown in Fig. 3c);
- the dielectric constant of the shell which is obtained from Eq. (3); and
- the dielectric constant of the medium surrounding the HNs ($\varepsilon_m = \varepsilon_{ethanol} = 1.85$).

In this scheme, the f value is the only fitting parameter of the simulations.

The average size of the Ag NPs can also be estimated using Mie theory. The spectral position of the peak of the simulated extinction spectrum of a $D = 56$ nm Ag nanosphere dispersed in ethanol (Fig. 6, red curve) matches that of the Ag NPs sample (Fig. 6, black curve). The experimental curve is considerably broader than the theoretical one, which is attributed to the size and shape distribution of the Ag NPs; however, it could be argued that such a distribution is predominantly composed by quasi-spherical Ag NPs mean size of which is 56 nm, which is in agreement with the TEM micrographs shown in Fig. 2b and the histogram shown in Fig. 2c. To model the extinction spectra of the Ag@ZnO core–shell HNs

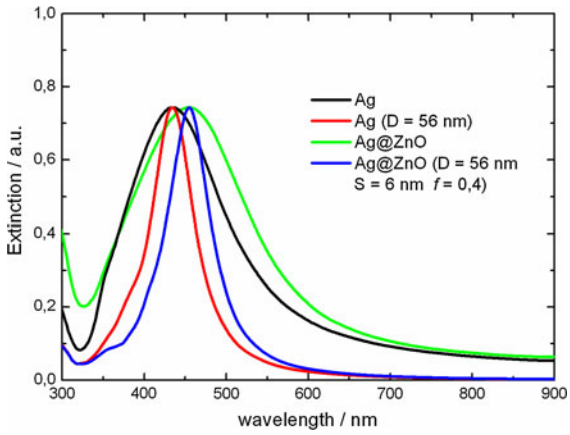

Fig. 6 Correlation between measured and simulated extinction spectra for Ag NPs and Ag@ZnO core–shell HNs

measured after 15 days aging, we have implemented the Mie theory for coated spheres with $D = 56$ nm, $S = 6$ nm (obtained from the histograms shown in Figs. 2c, 3c, respectively) and varying the f value. The spectrum obtained for $f = 0.4$ (Fig. 6, blue curve) fits very well the peak position of the experimental spectrum (Fig. 6, green curve). In this case, as before, the experimental spectrum is much broader than the theoretical one, which is attributed to the size and shape distribution, not only of the Ag NP cores but also of the shell thickness. It is important to emphasize the physical meaning of the value of the parameter $f = 0.4$. Considering that the maximum number (N) of spheres of diameter S that could be packed on the surface of a bigger sphere of diameter D is given by $N = \frac{2\pi}{\sqrt{3}}\left(1 + \frac{D}{S}\right)^2$ in the limit $D \gg S$, the maximum possible value for f is 0.6 for the present geometry. The comparison with this number indicates that the value $f = 0.4$ is reasonable, and it corresponds to a Ag sphere covered by a dense shell of ZnO QDs. Thus, the results shown in Fig. 6 support the interpretation that the redshift of the LSPR is a consequence of the formation of a ZnO QDs shell around a Ag NP and demonstrate that the sphere-coated models employed along with the average dielectric constant (Eq.(3)) are able to describe not only qualitatively but also quantitatively the extinction properties of Ag@ZnO core–shell NHs.

In order to qualitatively analyze the effects of the structural parameters of the HNs on its optical response, we have performed further simulations. Figure 7a shows the effect of increasing the shell thickness on the extinction spectra of a Ag@ZnO core–shell HNs by keeping the f value constant at 0.4. As the thickness of the shell increases from 0 to 10 nm, it is observed that the LSPR peak shifts from 435 to 463 nm, which is attributed to an increase of the ratio between the shell volume to the core volume. In addition, note that as the shell thickness is increased, a peak around 350 nm becomes more defined, which is attributed to absorption by ZnO. Instead, Fig. 7b displays the effects of increasing the f value on the extinction spectra of a Ag@ZnO core–shell nanostructure by keeping the shell thickness constant at 6 nm. Qualitatively, the same effects as in the previous case are observed, which are attributed to an increase of the effective dielectric constant. However, the changes are more pronounced; for instance, the peak

redshifts 45 nm (from 435 to 480 nm) when f is increased from 0 to 0.6. In addititon, the absorption peak around 350 nm is even more evident than in the previous example. Therefore, in general, the results shown in Fig. 7 indicate that, as expected, the LSPR redshifts as well as the absorption peak around 350 nm becomes more pronounced when increasing both the shell thickness and the volume fraction f.

Formation and growth mechanism of the HNs

Considering the evolution of the extinction spectra shown in Fig. 3a, it is possible to propose the following mechanism for the formation and growth of the HNs. Initially, a given number of small ZnO nucleus, which are rapidly formed from the bulk of the solution when the precursors are mixed, attach to the Ag NPs surface via COOH interactions; this number of ZnO nucleus attached on the Ag NPs surface remains nearly constant, but their size already increases with the aging time. This mechanism leads to a shell with increasing thickness and greater f values with lapse of time (see scheme in Fig. 8). As is shown in Fig. 7, increases in both the thickness and the f value produce a redshift in the LPSR, the same effect that is qualitatively observed in Fig. 3a. As we will show later, the model employed is also able to describe quantitatively the time evolution of the extinction spectra according to the proposed mechanism.

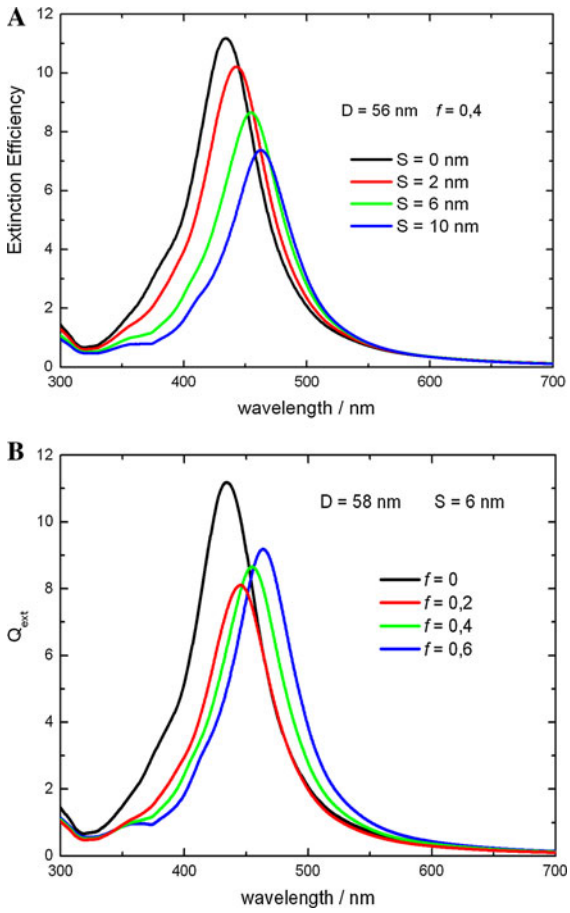

Fig. 7 Effect of **a** shell thickness and **b** volume fraction f on the simulated extinction spectrum of Ag@ZnO core–shell HNs

By calculating the volume of a shell of 6-nm thickness, corresponding to 15 days aging (see Fig. 3b and the histogram shown in Fig. 3c), and knowing the respective value of $f = 0.4$ and the volume of an individual 6.0 nm diameter ZnO QD, it is possible to estimate the average number of ZnO QDs that constitute the shell over a 56-nm diameter Ag NP, which, in this case, is equal to 274 ZnO QDs/Ag NP. Assuming that the global rate growth of ZnO QDs is the same irrespective of whether they are attached or not to the Ag NPs surface, it is possible to estimate that the average diameter of ZnO QDs in the Ag@ZnO HN for 7 days aging is the same as that determined for the green curve in Fig. 1a, i.e., 5.6 nm. Similar to the previous calculation, by estimating the shell thickness (5.6 nm), the number (274), and volume of each ZnO QD, it is possible to calculate the value of the parameter f for 7 days' aging time, which in this case gives $f = 0.35$. Interestingly, the peak of the extinction spectrum simulated with these new parameters match very well with the Ag@ZnO sample after 7 days' aging time (see blue curve in Fig. 9; Table 2). When repeating this procedure for 2 days' aging time, using a shell thickness of 5.0 nm, the volume fraction should be $f = 0.29$; while for 0.1-day aging time, with a shell thickness of 4.6 nm, the calculation gives $f = 0.25$. This analysis indicates that, as expected, decreasing the size of the ZnO QDs that constitute the shell and keeping constant its number, a decrease in the f values is obtained. The extinction spectra of the coated spheres simulated with the parameters obtained as described above for each aging time are plotted in Fig. 9. It can clearly be observed that these spectra follow the same trend with aging time as that the measured spectra for the HNs showed in Fig. 3a. In addition, the LSPR peak positions of the simulated spectra show an excellent agreement with those values corresponding to the measured spectra as compared in

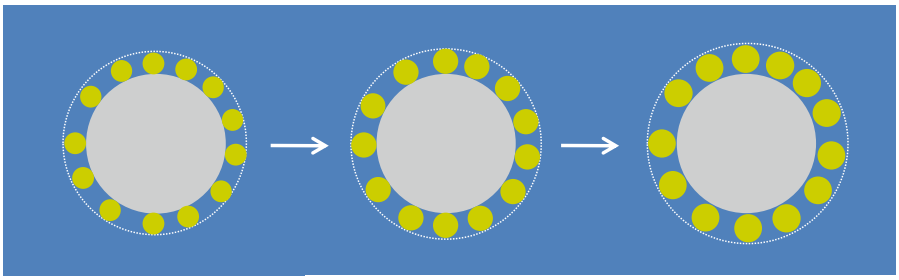

Fig. 8 Scheme of the proposed mechanism for the ZnO shell thickness growth

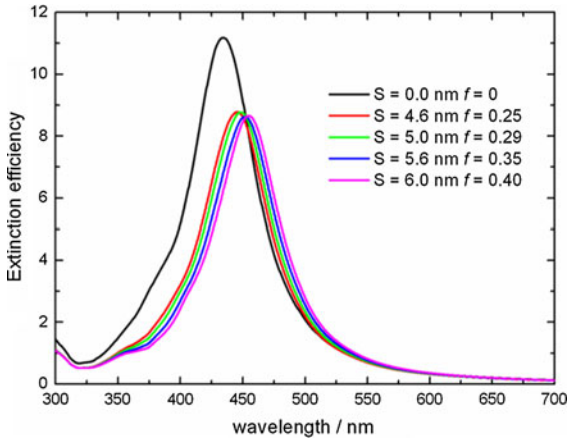

Fig. 9 Simulated extinction spectra for Ag@ZnO core–shell HNs at different aging times. The *S* and *f* values employed in each simulation obtained according to the purposed formation and growth mechanism are indicated in the *inset*. The spectrum of the core Ag nanosphere is also shown for comparative purposes

Table 2. These results support the mechanism proposed about the formation and growth of the Ag@ZnO core–shell HNs, pictorially shown in Fig. 8.

Finally, it is important to discuss how do the m_e^* m_h^* and ϵ values modify the results presented above. When the values reported by Pesika et al. (2002, 2003) are used in Eq. (2) to determine the size of the ZnO QDs, the results obtained do not show significant differences with those shown in Table 1 and follow the same trend (see Table 1S in Supporting Information). In turn, the *f* values obtained according to the purposed mechanism but using the ZnO QDs size values reported in Table 1S are quite similar to those shown in Fig. 9 (see Fig. 2S). Moreover, the LSPR peak positions of the simulated spectra shown in Fig. 1S are in good agreement with those values corresponding to the measured spectra as compared in Table 2S. This analysis indicates that the results presented in this study are only slightly modified according to the election of the m_e^*, m_h^* and ϵ values.

Table 2 Comparison between the peak positions of the extinction spectra λ_{LSPR} measured and simulated for Ag@ZnO HNs at different aging times

Aging time/days	0	0.1	2	7	15
$\lambda_{LSPR,\ measured}$/nm	435	443	447	452	455
$\lambda_{LSPR,\ simulated}$/nm	435	445	448	452	455

The values for 0 day aging time correspond to the unmodified Ag NPs

Conclusions

In summary, we have implemented a simple synthetic methodology which allows us to obtain Ag@ZnO core–shell HNs. At variance with most of the methodologies reported for the preparation of Ag–ZnO HNs, which account for relatively complex ZnO structures with dimensions on the order of several hundreds of nm, the method presented in this study gives rise to the formation of Ag NPs surrounded by ZnO QDs shells with average thickness of 6 nm. The method is general in the sense that it can be applied, in principle, to any set of properly modified Ag NPs surface. By means of electrodynamics calculations based on Mie theory for coated spheres, and applying the Maxwell–Garnett effective medium theory to calculate the average dielectric constant of the shell, it was possible to describe both qualitatively and quantitatively the changes in the extinction spectra as a consequence of the ZnO shell formation over the Ag NP. By virtue of this accurate description, it was also possible to propose a mechanism for its formation and growth.

Acknowledgments The authors thank CONICET, FONCYT, and SECyT (UNC) for their financial supports. The authors thank Lic. Luis A. Pérez for his help in performing

computational simulations, and to Dra. Claudia Nome and Lic. Nicolás Passarelli for their assistance in performing TEM measurements.

References

Aguirre MA, Rodríguez HB, San Román E, Feldhoff A, Grela MA (2011) Ag@ZnO core shell nanoparticles formed by the timely reduction of Ag^+ ions and zinc acetate hydrolysis in *N*,*N*-dimethylformamide: mechanism of growth and photocatalytic properties. J Phys Chem C 115:24967–24974

Bohrem CF, Huffman DR (1983) Absorption and scattering of light by small particles. Wiley-Interscience, New York

Brus LE (1984) Electron–electron and electronhole interactions in small semiconductor crystallites: the size dependence of the lowest excited electronic state. J Chem Phys 80: 4403–4409

Chen Y, Munechika K, Jen-La Plante I, Munro AM, Skrabalak AM, Xia Y, Ginger DS (2008) Excitation enhancement of CdSe quantum dots by single metal nanoparticles. Appl Phys Lett 93:053106

Chen L, Xu J, Holmes JD, Morris MA (2010) A facile route to ZnO nanoparticle superlattices: synthesis, functionalization, and self-assembly. J Phys Chem C 114:2003–2011

Cheng C, Yan B, Wong SM, Li X, Zhou W, Yu T, Shen Z, Yu H, Fan HJ (2010) Fabrication and SERS performance of silver-nanoparticle-decorated Si/ZnO nanotrees in ordered arrays. ACS Appl Mater Interfaces 2:1824–1828

Cho S, Jang J, Jung S, Lee BR, Oh E, Lee K (2009) Precursor effects of citric acid and citrates on ZnO crystal formation. Langmuir 25:3825–3831

Cohen-Hoshen E, Bryant G, Pinkas I, Sperling J, Bar-Joseph I (2012) Exciton–plasmon interactions in quantum dot–gold nanoparticle structures. Nano Lett 12:4260–4264

Costi R, Saunders AE, Banin U (2010) Colloidal hybrid nanostructures: a new type of functional materials. Angew Chem Int Ed 49:4878–4897

Encina ER, Coronado EA (2007) Resonance conditions for multipole plasmon excitations in noble metal nanorods. J Phys Chem C 111:16796–16801

Encina ER, Coronado EA (2010) Plasmon coupling in silver nanosphere pairs. J Phys Chem C 114:3918–3923

Fan F, Ding Y, Liu D, Tian Z, Wang ZL (2009) Facet-selective epitaxial growth of heterogeneous nanostructures of semiconductor and metal: ZnO nanorods on Ag nanocrystals. J Am Chem Soc 131:12036–12037

Georgekutty R, Seery MK, Pillai SC (2008) A highly efficient Ag–ZnO photocatalyst: synthesis, properties, and mechanism. J Phys Chem C 112:13563–13570

Hartlieb KJ, Raston CL, Saunders M (2007) Controlled scalable synthesis of ZnO nanoparticles. Chem Mater 19:5453–5459

Jakob M, Levanon H, Kamat PV (2003) Charge distribution between UV-irradiated TiO2 and gold nanoparticles: determination of shift in the Fermi level. Nano Lett 3:353–358

Jones MR, Osberg KD, Macfarlane RJ, Langille MR, Mirkin CA (2011) Templated techniques for the synthesis and assembly of plasmonic nanostructures. Chem Rev 111:3736–3827

Kamat PV (2012) Manipulation of charge transfer across semiconductor interface. A criterion that cannot be ignored in photocatalyst design. J Phys Chem Lett 3:663–672

Kelly KL, Coronado EA, Zhao LL, Schatz GC (2003) The optical properties of metal nanoparticles: the influence of size, shape, and dielectric environment. J Phys Chem B 107:668–677

Khanal BP, Pandey A, Li L, Lin Q, Bae WK, Luo H, Klimov VI, Pietryga JM (2012) Generalized synthesis of hybrid metal-semiconductor nanostructures tunable from the visible to the infrared. ACS Nano 6:3832–3840

Layek A, Mishra G, Sharma A, Spasova M, Dhar S, Chowdhury A, Bandyopadhyaya R (2012) A generalized three-stage mechanism of ZnO nanoparticle formation in homogeneous liquid medium. J Phys Chem C 116:24757–24769

Lee M, Kim TG, Kim W, Sung Y (2008) Surface plasmon resonance (SPR) electron and energy transfer in noble metal-zinc oxide composite nanocrystals. J Phys Chem C 112:10079–10082

Lee J, Shim HS, Lee M, Song JK, Lee D (2011) Size-controlled electron transfer and photocatalytic activity of ZnO–Au nanoparticle composites. J Phys Chem Lett 2:2840–2845

Lenz A, Selegard L, Soederlind F, Larsson A, Holtz PO, Uvdal K, Ojamae L, Kall P (2009) ZnO nanoparticles functionalized with organic acids: an experimental and quantum-chemical study. J Phys Chem C 113:17332–17341

Li M, Cushing SK, Wang Q, Shi X, Hornak LA, Hong Z, Wu N (2011) Size-dependent energy transfer between CdSe/ZnS quantum dots and gold nanoparticles. J Phys Chem Lett 2:2125–2129

Lin D, Wu H, Zhang R, Pan W (2009) Enhanced photocatalysis of electrospun Ag–ZnO heterostructured nanofibers. Chem Mater 21:3479–3484

Linic S, Christopher P, Ingram DV (2011) Plasmonic-metal nanostructures for efficient conversion of solar to chemical energy. Nat Mater 10:911–921

Liu D, Ding S, Lin H, Liu B, Ye Z, Fan F, Ren B, Tian Z (2012a) Distinctive enhanced and tunable plasmon resonant absorption from controllable Au@Cu2O nanoparticles: experimental and theoretical modeling. J Phys Chem C 116:4477–4483

Liu H, Shao GX, Zhao JF, Zhang ZX, Zhang Y, Liang J, Liu XG, Jia HS, Xu BS (2012b) Worm-like Ag/ZnO core–shell heterostructural composites: fabrication, characterization, and photocatalysis. J Phys Chem C 116:16182–16190

Lu W, Gao S, Wang J (2008) One-pot synthesis of Ag/ZnO self-assembled 3D hollow microspheres with enhanced photocatalytic performance. J Phys Chem C 112:16792–16800

Mahanti M, Basak D (2012) Highly enhanced UV emission due to surface plasmon resonance in Ag–ZnO nanorods. Chem Phys Lett 542:110–116

Meulenkamp EA (1998) Synthesis and growth of ZnO nanoparticles. J Phys Chem B 102:5566–5572

Munechika K, Chen Y, Tillack AF, Kulkarni AP, Jen-La Plante I, Munro AM, Ginger DS (2010) Spectral control of plasmonic emission enhancement from quantum dots near single silver nanoprisms. Nano Lett 10:2598–2603

Palik ED (1985) Handbook of optical constant of solids. Academic Press, New York

Pesika NS, Hu Z, Stebe KJ, Searson PC (2002) Quenching of growth of ZnO nanoparticles by adsorption of octanethiol. J Phys Chem B 106:6985–6990

Pesika NS, Stebe KJ, Searson PC (2003) Determination of the particle size distribution of quantum nanocrystals from absorption spectra. Adv Mater 15:1289–1291

Postava K, Sueki H, Aoyama M, Yamaguchi T, Ino C, Igasaki Y, Horie M (2000) Spectroscopic ellipsometry of epitaxial ZnO layer on sapphire substrate. J Appl Phys 87:7820–7824

Qi J, Dang X, Hammond PT, Belcher AM (2011) Highly efficient plasmon-enhanced dye-sensitized solar cells through metal@-oxide core–shell nanostructure. ACS Nano 5:7108–7116

Richter AP, Lombardi JR, Zhao B (2010) Size and wavelength dependence of the charge-transfer contributions to surface-enhanced Raman spectroscopy in Ag/PATP/ZnO junctions. J Phys Chem C 114:1610–1614

Rycenga M, Cobley CM, Zeng J, Li W, Moran CH, Zhang Q, Qin D, Xia Y (2011) Controlling the synthesis and assembly of silver nanostructures for plasmonic applications. Chem Rev 111:3669–3712

Segets D, Gradl J, Taylor RK, Vassilev V, Peukert W (2009) Analysis of optical absorbance spectra for the determination of ZnO nanoparticle size distribution, solubility, and surface energy. ACS Nano 3:1703–1710

Shan G, Xu L, Wang G, Liu Y (2007) Enhanced Raman scattering of ZnO quantum dots on silver colloids. J Phys Chem C 111:3290–3293

Subramanian V, Wolf E, Kamat PV (2003) Green emission to probe photoinduced charging events in ZnO–Au nanoparticles. Charge distribution and Fermi-level equilibration. J Phys Chem B 107:7479–7485

Sun Z, Yang Z, Zhou J, Yeung MH, Ni W, Wu H, Wang J (2009) A general approach to the synthesis of gold-metal sulfide core–shell and heterostructures. Angew Chem Int Ed 48: 2881–2885

Sun F, Tan F, Wanga W, Qiao X, Qiu X (2012) Facile synthesis of Ag/ZnO heterostructure nanocrystals with enhanced photocatalytic performance. Mater Res Bull 47:3357–3361

Taratula O, Galoppini E, Wang D, Chu D, Zhang Z, Chen H, Saraf G, Lu G (2006) Binding studies of molecular linkers to ZnO and MgZnO nanotip films. J Phys Chem B 110: 6506–6515

Torimoto T, Horibe H, Kameyama T, Okazaki K, Ikeda S, Matsumura M, Ishikawa A, Ishihara H (2011) Plasmon-enhanced photocatalytic activity of cadmium sulfide nanoparticle immobilized on silica-coated gold particles. J Phys Chem Lett 2:2057–2062

Udawatte N, Lee M, Kim J, Lee D (2011) Well-defined Au/ZnO nanoparticle composites exhibiting enhanced photocatalytic activities. ACS Appl Mater Interfaces 3:4531–4538

Viste P, Plain J, Jaffiol R, Vial A, Adam PM, Royer P (2010) Enhancement and quenching regimes in metal-semiconductor hybrid optical nanosources. ACS Nano 4:759–764

Wood A, Giersig M, Mulvaney P (2001) Fermi level equilibration in quantum dot-metal nanojunctions. J Phys Chem B 105:8810–8815

Xu F, Zhang Y, Sun Y, Shi Y, Wen Z, Li Z (2011) Silver nanoparticles coated zinc oxide nanorods array as superhydrophobic substrate for the amplified SERS effect. J Phys Chem C 115:9977–9983

Yoo D, Cuong TV, Luan VH, Khoa NT, Kim EJ, Hur SH, Hahn SH (2012) Photocatalytic performance of a Ag/ZnO/CCG multidimensional heterostructure prepared by a solution-based method. J Phys Chem C 116:7180–7184

Zhang J, Tang J, Lee K, Ouyang M (2010a) Nonepitaxial growth of hybrid core–shell nanostructures with large lattice mismatches. Science 327:1634–1638

Zhang L, Yin L, Wang C, Iun N, Qi Y, Xiang D (2010b) Origin of visible photoluminescence of ZnO quantum dots: defect-dependent and size-dependent. J Phys Chem C 114: 9651–9658

Zhang L, Blom DA, Wang H (2011a) Au–Cu2O core–shell nanoparticles: a hybrid metal-semiconductor heteronanostructure with geometrically tunable optical properties. Chem Mater 23:4587–4598

Zhang N, Liu S, Fu X, Xu Y (2011b) Synthesis of M@TiO2 (M = Au, Pd, Pt) core–shell nanocomposites with tunable photoreactivity. J Phys Chem C 115:9136–9145

Zheng Y, Zheng L, Zhan Y, Lin X, Zheng Q, Wei K (2007) Ag/ZnO heterostructure nanocrystals: synthesis, characterization, and photocatalysis. Inorg Chem 6:6980–6986

Zheng Y, Chen C, Zhan Y, Lin X, Zheng Q, Wei K, Zhu J (2008) Photocatalytic activity of Ag/ZnO heterostructure nanocatalyst: correlation between structure and property. J Phys Chem C 112:10773–10777